

# Measurement of the branching fractions for Cabibbo-suppressed decays

$$D^+ \rightarrow K^+ K^- \pi^+ \pi^0 \text{ and } D_{(s)}^+ \rightarrow K^+ \pi^- \pi^+ \pi^0 \text{ at Belle}$$

L. K. Li , A. J. Schwartz , K. Kinoshita , E. Won , H. Aihara , S. Al Said , D. M. Asner , H. Atmacan , V. Aulchenko , T. Aushev , R. Ayad , V. Babu , S. Bahinipati , K. Belous , J. Bennett , M. Bessner , V. Bhardwaj , T. Bilka , A. Bobrov , D. Bodrov , G. Bonvicini , J. Borah , A. Bozek , M. Bračko , P. Branchini , T. E. Browder , A. Budano , M. Campajola , D. Červenkov , P. Chang , A. Chen , B. G. Cheon , H. E. Cho , K. Cho , S.-J. Cho , S.-K. Choi , Y. Choi , S. Choudhury , D. Cinabro , S. Cunliffe , S. Das , N. Dash , G. De Nardo , G. De Pietro , R. Dhamija , F. Di Capua , Z. Doležal , T. V. Dong , D. Dossett , D. Epifanov , A. Frey , B. G. Fulsom , R. Garg , V. Gaur , A. Garmash , A. Giri , P. Goldenzweig , E. Graziani , D. Greenwald , T. Gu , Y. Guan , K. Gudkova , C. Hadjivasiliou , K. Hayasaka , H. Hayashii , D. Herrmann , W.-S. Hou , C.-L. Hsu , K. Inami , A. Ishikawa , R. Itoh , M. Iwasaki , W. W. Jacobs , S. Jia , Y. Jin , D. Kalita , A. B. Kaliyar , K. H. Kang , T. Kawasaki , C. Kiesling , C. H. Kim , D. Y. Kim , K.-H. Kim , K. T. Kim , Y.-K. Kim , P. Kodyš , T. Konno , A. Korobov , S. Korpar , E. Kovalenko , P. Križan , P. Krokovny , T. Kuhr , M. Kumar , R. Kumar , K. Kumara , A. Kuzmin , Y.-J. Kwon , Y.-T. Lai , T. Lam , M. Laurenza , S. C. Lee , J. Li , Y. Li , Y. B. Li , L. Li Gioi , J. Libby , K. Lieret , D. Liventsev , A. Martini , M. Masuda , T. Matsuda , D. Matvienko , S. K. Maurya , F. Meier , M. Merola , F. Metzner , K. Miyabayashi , R. Mizuk , G. B. Mohanty , H. K. Moon , M. Nakao , Z. Natkaniec , A. Natchii , L. Nayak , M. Nayak , N. K. Nisar , S. Nishida , H. Ono , P. Oskin , P. Pakhlov , G. Pakhlova , S. Pardi , H. Park , S.-H. Park , A. Passeri , S. Patra , S. Paul , T. K. Pedlar , R. Pestotnik , L. E. Piiilonen , T. Podobnik , E. Prencipe , M. T. Prim , A. Rostomyan , N. Rout , G. Russo , D. Sahoo , S. Sandilya , A. Sangal , L. Santelj , V. Savinov , G. Schnell , J. Schueler , C. Schwanda , Y. Seino , K. Senyo , M. E. Sevier , M. Shapkin , C. Sharma , J.-G. Shiu , F. Simon , J. B. Singh , A. Sokolov , E. Solovieva , M. Starič , Z. S. Stottler , M. Sumihama , M. Takizawa , U. Tamponi , K. Tanida , F. Tenchini , M. Uchida , T. Uglov , K. Uno , S. Uno , Y. Ushiroda , Y. Usov , R. van Tonder , G. Varner , K. E. Varvell , A. Vossen , E. Waheed , E. Wang , M.-Z. Wang , X. L. Wang , S. Watanuki , O. Werbycka , J. Wiechczynski , B. D. Yabsley , W. Yan , S. B. Yang , H. Ye , J. Yelton , J. H. Yin , C. Z. Yuan , Z. P. Zhang , V. Zhilich , and V. Zhukova 

(The Belle Collaboration)

We present measurements of the branching fractions for the singly Cabibbo-suppressed decays  $D^+ \rightarrow K^+ K^- \pi^+ \pi^0$  and  $D_s^+ \rightarrow K^+ \pi^- \pi^+ \pi^0$ , and the doubly Cabibbo-suppressed decay  $D^+ \rightarrow K^+ \pi^- \pi^+ \pi^0$ , based on 980 fb<sup>-1</sup> of data recorded by the Belle experiment at the KEKB  $e^+e^-$  collider. We measure these modes relative to the Cabibbo-favored modes  $D^+ \rightarrow K^- \pi^+ \pi^+ \pi^0$  and  $D_s^+ \rightarrow K^+ K^- \pi^+ \pi^0$ . Our results for the ratios of branching fractions are  $\mathcal{B}(D^+ \rightarrow K^+ K^- \pi^+ \pi^0)/\mathcal{B}(D^+ \rightarrow K^- \pi^+ \pi^+ \pi^0) = (11.32 \pm 0.13 \pm 0.26)\%$ ,  $\mathcal{B}(D^+ \rightarrow K^+ \pi^- \pi^+ \pi^0)/\mathcal{B}(D^+ \rightarrow K^- \pi^+ \pi^+ \pi^0) = (1.68 \pm 0.11 \pm 0.03)\%$ , and  $\mathcal{B}(D_s^+ \rightarrow K^+ \pi^- \pi^+ \pi^0)/\mathcal{B}(D_s^+ \rightarrow K^+ K^- \pi^+ \pi^0) = (17.13 \pm 0.62 \pm 0.51)\%$ , where the uncertainties are statistical and systematic, respectively. The second value corresponds to  $(5.83 \pm 0.42) \times \tan^4 \theta_C$ , where  $\theta_C$  is the Cabibbo angle; this value is larger than other measured ratios of branching fractions for a doubly Cabibbo-suppressed charm decay to a Cabibbo-favored decay. Multiplying these results by world average values for  $\mathcal{B}(D^+ \rightarrow K^- \pi^+ \pi^+ \pi^0)$  and  $\mathcal{B}(D_s^+ \rightarrow K^+ K^- \pi^+ \pi^0)$  yields  $\mathcal{B}(D^+ \rightarrow K^+ K^- \pi^+ \pi^0) = (7.08 \pm 0.08 \pm 0.16 \pm 0.20) \times 10^{-3}$ ,  $\mathcal{B}(D^+ \rightarrow K^+ \pi^- \pi^+ \pi^0) = (1.05 \pm 0.07 \pm 0.02 \pm 0.03) \times 10^{-3}$ , and  $\mathcal{B}(D_s^+ \rightarrow K^+ \pi^- \pi^+ \pi^0) = (9.44 \pm 0.34 \pm 0.28 \pm 0.32) \times 10^{-3}$ , where the third uncertainty is due to the branching fraction of the normalization mode. The first two results are consistent with, but more precise than, the current world averages. The last result is the first measurement of this branching fraction.

## I. INTRODUCTION

Cabibbo-suppressed (CS) hadronic decays of charm mesons provide a powerful means to search for new physics [1]. Because such decays are suppressed in the Standard Model, their decay rates are especially sensitive to small new-physics contributions to the am-

plitudes. Thus, it is important to measure such decays with high precision. It is notable that the only observation of  $CP$  violation in charm decays, possibly arising from new physics [1], was made with the singly Cabibbo-suppressed (SCS) decays  $D^0 \rightarrow K^+ K^-$  and  $D^0 \rightarrow \pi^+ \pi^-$  [2]. Experimentally, CS decays can be challenging to measure, as they typically have higher

background levels than those for Cabibbo-favored (CF) decays.

In this paper, we present measurements of the branching fractions for the SCS decays  $D^+ \rightarrow K^+ K^- \pi^+ \pi^0$  and  $D_s^+ \rightarrow K^+ \pi^- \pi^+ \pi^0$ , and the doubly Cabibbo-suppressed (DCS) decay  $D^+ \rightarrow K^+ \pi^- \pi^+ \pi^0$ . Throughout this paper, charge-conjugate modes are implicitly included. The branching fractions are measured relative to those for the well-measured CF modes  $D^+ \rightarrow K^- \pi^+ \pi^+ \pi^0$  and  $D_s^+ \rightarrow K^+ K^- \pi^+ \pi^0$ . The branching fraction of a DCS decay relative to its CF counterpart is expected to be approximately  $\tan^4 \theta_C = 0.29\%$  [3], where  $\theta_C$  is the Cabibbo angle. The SCS decay  $D^+ \rightarrow K^+ K^- \pi^+ \pi^0$ , and the DCS decay  $D^+ \rightarrow K^+ \pi^- \pi^+ \pi^0$ , were recently observed by the BESIII experiment [4–6]. The decay  $D_s^+ \rightarrow K^+ \pi^- \pi^+ \pi^0$  has not yet been observed. The average of the absolute branching fractions measured at BESIII [5, 6] is  $\mathcal{B}(D^+ \rightarrow K^+ \pi^- \pi^+ \pi^0) = (1.18 \pm 0.07) \times 10^{-3}$ ; this gives a ratio of branching fractions  $\mathcal{B}(D^+ \rightarrow K^+ \pi^- \pi^+ \pi^0) / \mathcal{B}(D^+ \rightarrow K^- \pi^+ \pi^+ \pi^0) = (1.89 \pm 0.12)\%$ , which corresponds to  $(6.56 \pm 0.42) \times \tan^4 \theta_C$ . This value is larger than other measured ratios of DCS to CF branching fractions, which are in the range  $(0.7\text{--}1.8) \times \tan^4 \theta_C$  [7]. To investigate this further, we use the full Belle data set to measure these decay modes with high precision.

## II. DETECTOR AND DATA SET

Our analysis uses the full data set of the Belle experiment, which corresponds to an integrated luminosity of  $980 \text{ fb}^{-1}$  collected at or near the  $\Upsilon(nS)$  ( $n = 1, 2, 3, 4, 5$ ) resonances. The Belle experiment ran at the KEKB asymmetric-energy  $e^+e^-$  collider [8, 9]. The Belle detector is a large-solid-angle magnetic spectrometer consisting of a silicon vertex detector (SVD), a 50-layer central drift chamber (CDC), an array of aerogel threshold Cherenkov counters (ACC), a barrel-like arrangement of time-of-flight scintillation counters (TOF), and an electromagnetic calorimeter (ECL) comprising CsI(Tl) crystals located inside a superconducting solenoid coil providing a 1.5 T magnetic field. An iron flux-return located outside the coil is instrumented to detect  $K_L^0$  mesons and to identify muons (KLM). A detailed description of the detector is given in Ref. [9, 10].

We use Monte Carlo (MC) simulated events to optimize selection criteria, study sources of background, and calculate selection efficiencies. Signal MC events are generated using EVTGEN [11] and propagated through a detector simulation based on GEANT3 [12]. Final-state radiation from charged particles is simulated using PHOTOS [13]. Four-body decays are generated to decay uniformly in phase space without intermediate resonances. An MC sample of generic  $e^+e^-$  collisions corresponding to the same integrated luminosity as the data sample is

used to develop selection criteria.

## III. EVENT SELECTION

To ensure that tracks are well reconstructed, each final-state charged particle is required to have at least two SVD hits in each of the longitudinal and azimuthal measuring coordinates. Charged particles are identified by calculating likelihoods  $\mathcal{L}_i$  for specific particle hypotheses, where  $i = \pi, K, p, \mu, e$ . These likelihoods are based on information from various detectors: photon yield in the ACC,  $dE/dx$  information from the CDC, time-of-flight information from the TOF, energy in the ECL, and hits in the KLM [14–16]. Tracks with  $\mathcal{L}_K / (\mathcal{L}_K + \mathcal{L}_\pi) > 0.6$  are identified as kaon candidates; otherwise, tracks are considered pion candidates. Kaon candidates must also satisfy  $\mathcal{L}_p / (\mathcal{L}_p + \mathcal{L}_K) < 0.95$ . Tracks that satisfy  $\mathcal{L}_e / (\mathcal{L}_e + \mathcal{L}_{\text{hadron}}) > 0.95$  or  $\mathcal{L}_\mu / (\mathcal{L}_\mu + \mathcal{L}_\pi + \mathcal{L}_K) > 0.95$  are rejected, where  $\mathcal{L}_e$ ,  $\mathcal{L}_{\text{hadron}}$ , and  $\mathcal{L}_\mu$  are determined mainly using information from the ECL and KLM detectors [15, 16]. These requirements have an efficiency of about 90% for kaons and 95% for pions.

Photon candidates are identified from energy clusters in the ECL that are not associated with any charged track. The photon energy is required to be greater than 50 MeV in the barrel region (covering the polar angle  $32^\circ < \theta < 129^\circ$ ), and greater than 100 MeV in the end-cap region (covering  $12^\circ < \theta < 31^\circ$  or  $132^\circ < \theta < 157^\circ$ ). The ratio of the energy deposited in the  $3 \times 3$  array of crystals centered on the crystal with the highest energy, to the energy deposited in the corresponding  $5 \times 5$  array of crystals, is required to be greater than 0.80. Candidate  $\pi^0 \rightarrow \gamma\gamma$  decays are reconstructed from photon pairs having an invariant mass satisfying  $115 \text{ MeV}/c^2 < M(\gamma\gamma) < 150 \text{ MeV}/c^2$ ; this region corresponds to about  $3\sigma$  in  $M(\gamma\gamma)$  resolution.

A  $D_{(s)}^+$  candidate is reconstructed by combining  $K^- K^+ \pi^+$  or  $K^\pm \pi^\mp \pi^+$  track combinations with a  $\pi^0$  candidate. A vertex fit is performed for the three charged tracks and its fit quality is defined as  $\chi_{\text{vtx}}^2$ . The coordinates of the fitted vertex are assigned as the  $D_{(s)}^+$  decay vertex position.

Final selection criteria are determined by maximizing a figure-of-merit (FOM), which is defined as either  $S/\sqrt{S+B}$  for  $D^+ \rightarrow K^+ K^- \pi^+ \pi^0$  and  $D^+ \rightarrow K^+ \pi^- \pi^+ \pi^0$  or  $S/\sqrt{B}$  for  $D_s^+ \rightarrow K^+ \pi^- \pi^+ \pi^0$ , where  $S$  and  $B$  are the numbers of signal and background events, respectively, expected in a region  $-30 \text{ MeV}/c^2 < M(D) - m_D < 20 \text{ MeV}/c^2$ . In this expression,  $M(D)$  is the invariant mass of a reconstructed  $D^+$  or  $D_s^+$  candidate, and  $m_D$  is the known  $D^+$  or  $D_s^+$  mass [7]. This region corresponds to about  $2.5\sigma$  in the  $M(D)$  resolution. The FOM for  $D_s^+ \rightarrow K^+ \pi^- \pi^+ \pi^0$  is different because the branching fraction for this mode has not yet been measured.

Pairs of  $\gamma$  candidates are subjected to a fit in which

the  $\gamma$ 's are constrained to originate from the  $D_{(s)}^+$  decay vertex, and their invariant mass is constrained to the nominal  $\pi^0$  mass [7]. The resulting fit quality ( $\chi_{\pi^0}^2$ ) is required to satisfy  $\chi_{\pi^0}^2 < 8$ . To improve the momentum resolution of the  $\pi^0$ , the  $\gamma$  energies are updated from this fit; the resulting  $\pi^0$  momentum is required to be greater than 0.40 GeV/ $c$ . We veto  $D_{(s)}^+ \rightarrow K^+\pi^-\pi^+\pi^0$  candidates satisfying  $|M(\pi^+\pi^-) - m_{K_S^0}| < 10$  MeV/ $c^2$ , where  $m_{K_S^0}$  is the nominal  $K_S^0$  mass [7], to suppress peaking backgrounds such as  $D_{(s)}^+ \rightarrow K^+K_S^0\pi^0$ . This region corresponds to about  $3\sigma$  in mass resolution.

The  $D_{(s)}^+$  production vertex is determined by fitting the  $D_{(s)}^+$  trajectory to the  $e^+e^-$  interaction point (IP), which is determined from the beam profiles. This vertex fit quality is defined as  $\chi_{\text{IP}}^2$ . The sum of vertex fit qualities  $\chi_{\text{vtx}}^2 + \chi_{\text{IP}}^2$  is required to be less than 14 for  $D^+ \rightarrow K^+K^-\pi^+\pi^0$  decays, and less than 10 for the other signal modes. This requirement has a signal efficiency of 80%–82% while rejecting 60%–80% of background.

The dominant source of background is random combinations of particles produced in  $e^+e^- \rightarrow c\bar{c}$  events or in  $B$  decays. To suppress this background, the momentum of the  $D^+$  or  $D_s^+$  candidate in the  $e^+e^-$  center-of-mass frame is required to be greater than 2.5 GeV/ $c$  or 2.9 GeV/ $c$ , respectively. To further suppress backgrounds, we calculate the significance of the  $D_{(s)}^+$  decay length  $L/\sigma_L$ , where  $L$  is the projection of the vector running from the production vertex to the  $D_{(s)}^+$  decay vertex onto the momentum direction. The corresponding uncertainty  $\sigma_L$  is calculated by propagating uncertainties in the vertices and the  $D_{(s)}^+$  momentum, including their correlations. We subsequently require  $L/\sigma_L > 4.0$  for  $D^+ \rightarrow K^+K^-\pi^+\pi^0$ ,  $L/\sigma_L > 9.0$  for  $D^+ \rightarrow K^+\pi^-\pi^+\pi^0$ , and  $L/\sigma_L > 2.5$  for  $D_s^+ \rightarrow K^+\pi^-\pi^+\pi^0$ . The resulting signal efficiencies are 58%–77%, while more than 93%–99.8% of background is rejected.

The CF normalization modes  $D^+ \rightarrow K^-\pi^+\pi^+\pi^0$  and  $D_s^+ \rightarrow K^+K^-\pi^+\pi^0$  are selected with the same criteria as those used to select the signal modes, to minimize systematic uncertainties. For both signal and normalization modes, we retain events that satisfy  $-70$  MeV/ $c^2 < M(D) - m_D < 60$  MeV/ $c^2$ .

After applying all selection criteria, about 10% of events for  $D^+$  decay modes and 15% of events for  $D_s^+$  decay modes have multiple signal candidates. For these events, the average multiplicity is about 2.2 candidates for each channel. We select a single candidate by choosing the one with the smallest value of the sum  $\chi_{\pi^0}^2 + \chi_{\text{vtx}}^2 + \chi_{\text{IP}}^2$ . Based on MC simulation, this criterion selects the correct signal candidate 68% of the time.

There are backgrounds from  $D^{*+}$  decays in which the final state particles are the same as those for the signal or normalization modes. These are as follows:

- for  $D^+ \rightarrow K^-h^+\pi^+\pi^0$  decays, where  $h^+ = K^+$

or  $\pi^+$ , there is background from  $D^{*+} \rightarrow D^0\pi^+$ ,  $D^0 \rightarrow K^-h^+\pi^0(\pi^0)$ . To reject this background, we require  $M(K^-h^+\pi^+\pi^0) - M(K^-h^+\pi^0) - m_{\pi^+} > 20$  MeV/ $c^2$ .

- for  $D_s^+ \rightarrow K^+K^-\pi^+\pi^0$ , there is background from  $D^{*+} \rightarrow D^0\pi^+$ ,  $D^0 \rightarrow K^-K^+\pi^0$ , and from  $D^{*+} \rightarrow D^+\pi^0$ ,  $D^+ \rightarrow K^-K^+\pi^+$ . To reject these, we require  $M(K^-K^+\pi^+\pi^0) - M(K^-K^+\pi^+) - m_{\pi^0} > 10$  MeV/ $c^2$ , and also  $M(K^-K^+\pi^+\pi^0) - M(K^-K^+\pi^0) - m_{\pi^+} > 10$  MeV/ $c^2$ .
- for  $D_{(s)}^+ \rightarrow K^+\pi^-\pi^+\pi^0$ , there is background from  $D^{*-} \rightarrow \bar{D}^0\pi^-$ ,  $\bar{D}^0 \rightarrow K^+\pi^-\pi^0$ , with the  $\pi^-$  replaced by a random  $\pi^+$ . To suppress this background, we require  $M(K^+\pi^-\pi^+\pi^0) - M(K^+\pi^+\pi^0) - m_{\pi^-} > 40$  MeV/ $c^2$ .

These requirements reject only 1%–3% of signal decays but reduce  $D^{*+}$  backgrounds to a negligible level.

#### IV. YIELD EXTRACTION

We determine signal yields by performing an extended unbinned maximum-likelihood fit to the  $M(D)$  distributions. The probability density function (PDF) describing signal decays is taken to be the sum of a Crystal Ball function [17] and three asymmetric Gaussians (AG), which are Gaussian functions with different widths on the left- and right-hand sides of the peak position. This position is denoted by the parameter  $\mu$ , and all four functions are required to have a common value of  $\mu$ . An additional term ( $\mathcal{P}_{\text{FSR}}$ ) is included to describe signal decays with final-state radiation (FSR). For this term, the sum of a CB function and a Gaussian is used; the parameters of  $\mathcal{P}_{\text{FSR}}$  and its ratio to the total signal yield ( $f_{\text{FSR}}$ ) are fixed to MC values. The overall PDF is

$$\begin{aligned} \mathcal{P}_{\text{sig}} = (1 - f_{\text{FSR}}) & \left[ f_3 \left[ f_2 \left[ f_1 \cdot \text{AG}(\mu, \sigma_1, \delta_1) \right. \right. \right. \\ & \left. \left. \left. + (1 - f_1) \cdot \text{AG}(\mu, \sigma_2, \delta_2) \right] \right. \right. \\ & \left. \left. + (1 - f_2) \cdot \text{AG}(\mu, \sigma_3, \delta_3) \right] \right. \\ & \left. + (1 - f_3) \cdot \text{CB}(\mu, \sigma_4, \alpha_{\text{cb}}, n_{\text{cb}}) \right] \\ & + f_{\text{FSR}} \cdot \mathcal{P}_{\text{FSR}}, \end{aligned} \quad (1)$$

where  $\sigma_{i+1} = r_i\sigma_i$  ( $i = 1, 2, 3$ ) with a scaling factor  $r_i$ , and the left-side ( $L$ ) and right-side ( $R$ ) widths of the asymmetric Gaussians are specified by the parameter  $\delta_i$ :  $\sigma_i^{L,R} = \sigma_i(1 \pm \delta_i)$ . The parameters  $\mu$  and  $\sigma_1$  are free to vary, which allows for a difference in resolution between data and MC simulation; all other parameters are fixed to MC values. The mode  $D^+ \rightarrow K^+\pi^-\pi^+\pi^0$  is fitted simultaneously with the normalization mode

$D^+ \rightarrow K^- \pi^+ \pi^+ \pi^0$ , as both modes share signal shape parameters.

The background shapes are described by second-order Chebyshev polynomials for  $D^+ \rightarrow K^+ \pi^- \pi^+ \pi^0$  and  $D_s^+ \rightarrow K^+ \pi^- \pi^+ \pi^0$ , and a third-order Chebyshev polynomial for  $D^+ \rightarrow K^+ K^- \pi^+ \pi^0$ . All parameters of these shapes are free to vary.

Projections of the  $M(D)$  fits are shown in Fig. 1 for  $D^+ \rightarrow K^+ K^- \pi^+ \pi^0$  and its normalization mode  $D^+ \rightarrow K^- \pi^+ \pi^+ \pi^0$ ; in Fig. 2 for  $D^+ \rightarrow K^+ \pi^- \pi^+ \pi^0$  and its normalization mode  $D^+ \rightarrow K^- \pi^+ \pi^+ \pi^0$ ; and in Fig. 3 for  $D_s^+ \rightarrow K^+ \pi^- \pi^+ \pi^0$  and its normalization mode  $D_s^+ \rightarrow K^+ K^- \pi^+ \pi^0$ . Also plotted are the pulls, defined as  $(N_{\text{data}} - N_{\text{fit}})/\sigma$ , where  $\sigma$  is the uncertainty on  $N_{\text{data}}$ . The pull distributions show that the fits describe the data satisfactorily. The signal and background yields ( $N_{\text{sig}}$  and  $N_{\text{bkg}}$ ) obtained from the fits for the signal region,  $\pm 20 \text{ MeV}/c^2$  around the nominal  $D_{(s)}^+$  mass, are listed in Table I.

The statistical significance of a signal yield is evaluated as the difference in the log likelihoods obtained from fits performed with and without a signal PDF. For  $D^+ \rightarrow K^+ \pi^- \pi^+ \pi^0$ , we obtain  $\Delta \ln \mathcal{L} = 177$ ; as the number of degrees of freedom for the fit without a signal component is one less than that with a signal component, this value corresponds to a statistical significance of greater than  $10\sigma$ . For  $D_s^+ \rightarrow K^+ \pi^- \pi^+ \pi^0$ , we obtain  $\Delta \ln \mathcal{L} = 594$ . In this case, the number of degrees of freedom without a signal component is three less than that with a signal component (parameters  $N_{\text{sig}}$ ,  $\mu$ , and  $\sigma_1$  are dropped), and this value of  $\Delta \ln \mathcal{L}$  corresponds to a statistical significance of greater than  $10\sigma$ . This measurement constitutes the first observation of this  $D_s^+$  decay.

## V. BRANCHING FRACTIONS

To determine the branching fractions, we divide the signal yields by their respective reconstruction efficiencies. However, the reconstruction efficiency for a decay can vary across the four-body phase space, and the distribution in phase space of these decays is unknown. To reduce systematic uncertainty arising from the unknown decay distribution (which often contains intermediate resonances), we correct the signal yields for reconstruction efficiencies in bins of phase space as follows.

For a  $D_{(s)}^+$  decay to four pseudoscalar particles in the final state, the phase space is five-dimensional (5D). We thus correct the data for acceptance and reconstruction efficiency in bins of 5D phase space, where the bins are taken to be the invariant masses squared of five pairs of final-state particles [19]. These are calculated from fits subject to the mass constraint  $M(D) = m_{D^+}$  or  $m_{D_s^+}$ . The reconstruction efficiency is determined. The

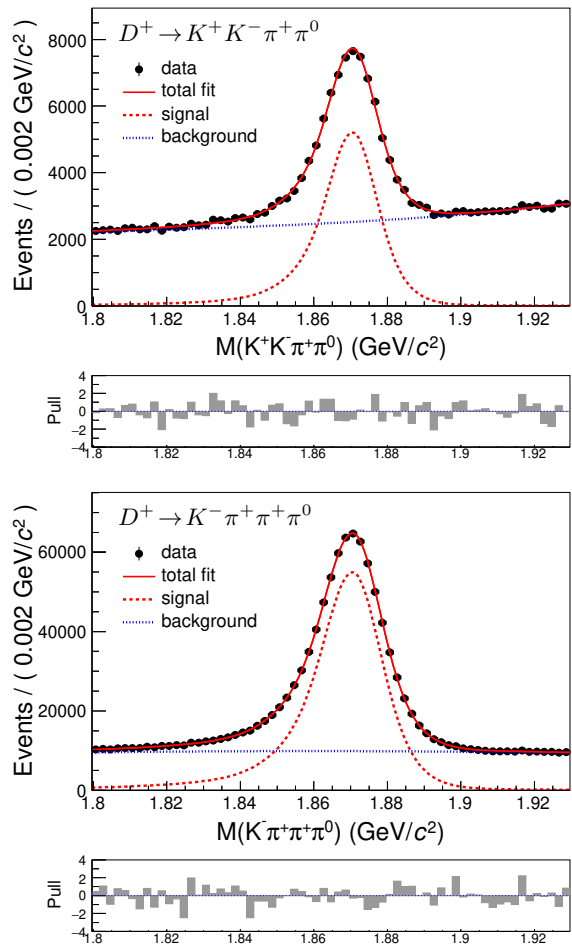


FIG. 1. Fit projections for  $D^+ \rightarrow K^+ K^- \pi^+ \pi^0$ , and its normalization mode  $D^+ \rightarrow K^- \pi^+ \pi^+ \pi^0$ . Data are plotted as filled circles with error bars. The red solid, red dashed, and blue dashed curves denote the overall fit result, the signal component, and the background component, respectively.

efficiency-corrected signal yield is calculated as

$$N_{\text{sig}}^{\text{corr}} = \sum_i \frac{N_i^{\text{data}} - N_{\text{bkg}} \cdot f_i^{\text{bkg}}}{\varepsilon_i}, \quad (2)$$

where  $N_i^{\text{data}}$ ,  $f_i^{\text{bkg}}$ , and  $\varepsilon_i$  are the number of data events, the fraction of background events, and the reconstruction efficiency for bin  $i$ . The summation runs over all bins. The uncertainties on each term in Eq. (2), for each bin  $i$ , are propagated to obtain the overall uncertainty on  $N_{\text{sig}}^{\text{corr}}$ . The bin sizes are chosen to minimize efficiency variations within the bins. There are 576 bins for  $D^+ \rightarrow K^+ K^- \pi^+ \pi^0$  (i.e.,  $4 \times 4 \times 3 \times 4 \times 3$ ); 243 bins for  $D^+ \rightarrow K^+ \pi^- \pi^+ \pi^0$ ; 768 bins for  $D^+ \rightarrow K^- \pi^+ \pi^+ \pi^0$ ; 432 bins for  $D_s^+ \rightarrow K^+ \pi^- \pi^+ \pi^0$ ; and 576 bins for  $D_s^+ \rightarrow K^+ K^- \pi^+ \pi^0$ . Invariant mass squared distributions for different combinations of final-state particles (i.e., projections of the five-dimensional distribution) are shown in Fig. 4 for  $D^+ \rightarrow K^+ K^- \pi^+ \pi^0$ , Fig. 5 for  $D^+ \rightarrow K^+ \pi^- \pi^+ \pi^0$ , and Fig. 6 for  $D_s^+ \rightarrow K^+ \pi^- \pi^+ \pi^0$ .

TABLE I. Fitted signal yields ( $N_{\text{sig}}$ ) and background yields ( $N_{\text{bkg}}$ ) in the region  $\pm 20 \text{ MeV}/c^2$  around the nominal  $D_{(s)}^+$  mass, and efficiency-corrected signal yields ( $N_{\text{sig}}^{\text{corr}}$ ) for (1)  $D^+ \rightarrow K^+ K^- \pi^+ \pi^0$ ; (2)  $D^+ \rightarrow K^+ \pi^- \pi^+ \pi^0$ ; and (3)  $D_s^+ \rightarrow K^+ \pi^- \pi^+ \pi^0$ . The normalization modes are  $D^+ \rightarrow K^- \pi^+ \pi^+ \pi^0$  for (1) and (2), and  $D_s^+ \rightarrow K^+ K^- \pi^+ \pi^0$  for (3). The  $N_{\text{sig}}$  values are not directly used to calculate  $N_{\text{sig}}^{\text{corr}}$ , which is calculated using Eq. (2). The normalization mode  $D^+ \rightarrow K^- \pi^+ \pi^+ \pi^0$  is used for both (1) and (2) but selected with different criteria in the two cases. Thus, the yields of this mode for (1) and (2) differ. Also listed are ratios of branching fractions (see text). The event yields are listed with their statistical uncertainty; the branching fraction ratios are listed with both statistical and systematic uncertainties. The right-most column lists the current world average (WA) [4–7].

	Decay mode	$N_{\text{sig}}$	$N_{\text{bkg}}$	$N_{\text{sig}}^{\text{corr}} (\times 10^6)$	Branching fraction ratio	Current WA
(1)	$D^+ \rightarrow K^+ K^- \pi^+ \pi^0$	$49\,798 \pm 564$	$50\,463 \pm 214$	$2.352 \pm 0.025$	$(11.32 \pm 0.13 \pm 0.26)\%$	$(10.6 \pm 0.6)\%$
	$D^+ \rightarrow K^- \pi^+ \pi^+ \pi^0$	$602\,463 \pm 1\,614$	$197\,151 \pm 570$	$20.77 \pm 0.07$		
(2)	$D^+ \rightarrow K^+ \pi^- \pi^+ \pi^0$	$3\,631 \pm 198$	$18\,879 \pm 101$	$0.303 \pm 0.020$	$(1.68 \pm 0.11 \pm 0.03)\%$	$(1.89 \pm 0.12)\%$
	$D^+ \rightarrow K^- \pi^+ \pi^+ \pi^0$	$208\,118 \pm 707$	$22\,327 \pm 212$	$18.06 \pm 0.10$		
(3)	$D_s^+ \rightarrow K^+ \pi^- \pi^+ \pi^0$	$26\,150 \pm 1\,442$	$277\,160 \pm 582$	$1.464 \pm 0.052$	$(17.13 \pm 0.62 \pm 0.51)\%$	...
	$D_s^+ \rightarrow K^+ K^- \pi^+ \pi^0$	$110\,261 \pm 735$	$71\,425 \pm 263$	$8.547 \pm 0.059$		

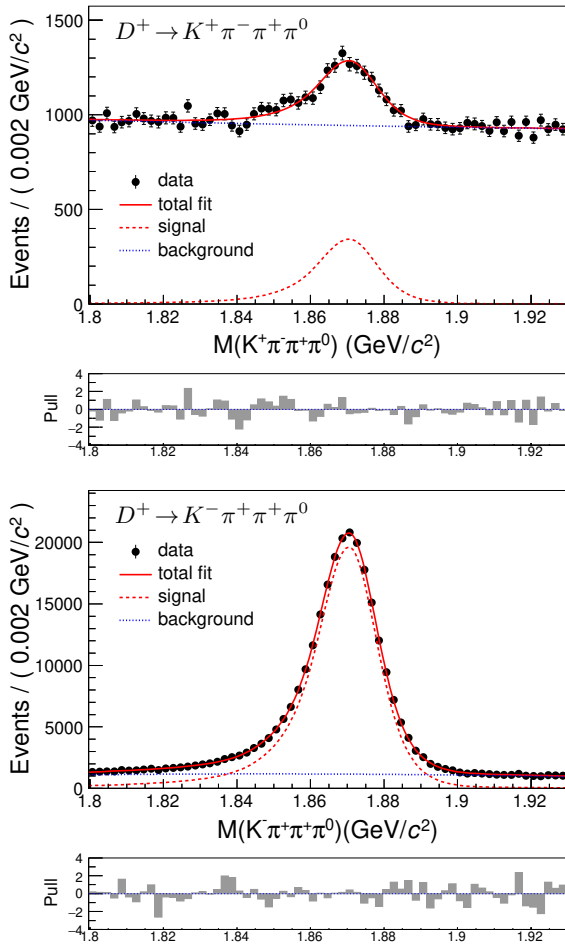


FIG. 2. Fit projections for  $D^+ \rightarrow K^+ \pi^- \pi^+ \pi^0$ , and its normalization mode  $D^+ \rightarrow K^- \pi^+ \pi^+ \pi^0$ . The signal PDFs are the same for the two modes (see text). Data are plotted as filled circles with error bars. The red solid, red dashed, and blue dashed curves denote the overall fit result, the signal component, and the background component, respectively.

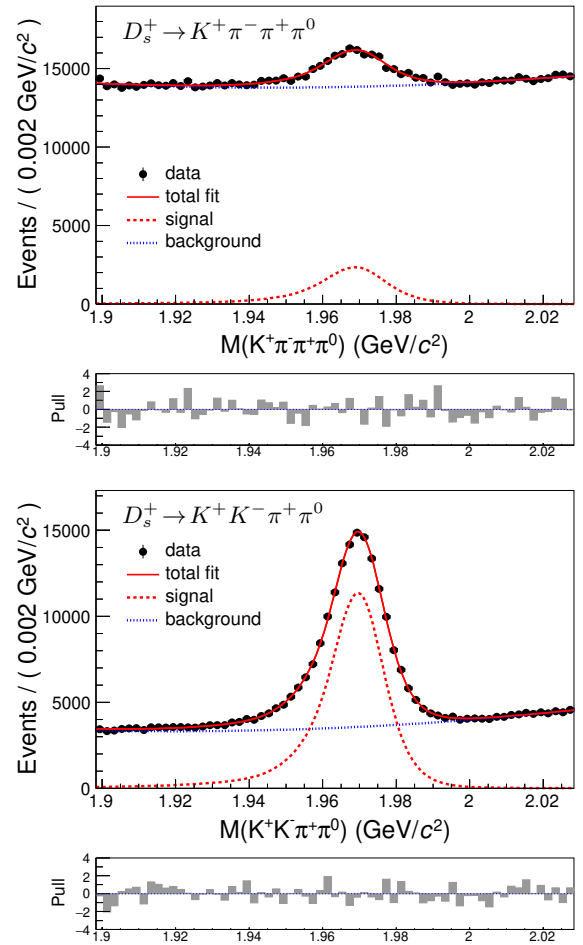


FIG. 3. Fit projections for  $D_s^+ \rightarrow K^+ \pi^- \pi^+ \pi^0$ , and its normalization mode  $D_s^+ \rightarrow K^+ K^- \pi^+ \pi^0$ . Data are plotted as filled circles with error bars. The red solid, red dashed, and blue dashed curves denote the overall fit result, the signal component, and the background component, respectively.

The reconstruction efficiencies  $\varepsilon_i$  are determined from a large sample of MC events. These efficiencies include a correction for particle identification, to account for small differences observed between data and MC simulation. The correction, typically 0.93–1.03, is determined from a sample of  $D^{*+} \rightarrow D^0\pi^+$ ,  $D^0 \rightarrow K^-\pi^+$  decays. The fraction of background events in the  $i$ th bin ( $f_i^{\text{bkg}}$ ) is obtained from the 5D distribution of events in the  $M(D)$  sidebands  $-70 \text{ MeV}/c^2 < M(D) - m_D < -50 \text{ MeV}/c^2$  and  $40 \text{ MeV}/c^2 < M(D) - m_D < 60 \text{ MeV}/c^2$ . An MC study shows that background in the signal region is well-described by background in the sidebands. The background fractions must satisfy the constraint  $\sum_i f_i^{\text{bkg}} = 1$ . The efficiency-corrected signal yields obtained using Eq. (2) are listed in Table I.

The ratio of the efficiency-corrected yield for a CS mode to that for a CF mode is equal to the ratio of branching fractions:  $N_{\text{sig}}^{\text{corr}}(\text{CS})/N_{\text{sig}}^{\text{corr}}(\text{CF}) = \mathcal{B}(\text{CS})/\mathcal{B}(\text{CF})$ . Inserting values from Table I, we obtain

$$\frac{\mathcal{B}(D^+ \rightarrow K^+K^-\pi^+\pi^0)}{\mathcal{B}(D^+ \rightarrow K^-\pi^+\pi^+\pi^0)} = (11.32 \pm 0.13)\% \quad (3)$$

$$\frac{\mathcal{B}(D^+ \rightarrow K^+\pi^-\pi^+\pi^0)}{\mathcal{B}(D^+ \rightarrow K^-\pi^+\pi^+\pi^0)} = (1.68 \pm 0.11)\% \quad (4)$$

$$\frac{\mathcal{B}(D_s^+ \rightarrow K^+\pi^-\pi^+\pi^0)}{\mathcal{B}(D_s^+ \rightarrow K^+K^-\pi^+\pi^0)} = (17.13 \pm 0.62)\%, \quad (5)$$

where the uncertainties listed are statistical.

## VI. SYSTEMATIC UNCERTAINTIES

Because we measure the ratio of branching fractions for decays with similar final states, most systematic uncertainties cancel. The remaining uncertainties are listed in Table II and evaluated as follows.

TABLE II. Fractional systematic uncertainties (in %) for the following ratios of branching fractions:

- (a)  $\mathcal{B}(D^+ \rightarrow K^+K^-\pi^+\pi^0)/\mathcal{B}(D^+ \rightarrow K^-\pi^+\pi^+\pi^0)$ ;  
 (b)  $\mathcal{B}(D^+ \rightarrow K^+\pi^-\pi^+\pi^0)/\mathcal{B}(D^+ \rightarrow K^-\pi^+\pi^+\pi^0)$ ; and  
 (c)  $\mathcal{B}(D_s^+ \rightarrow K^+\pi^-\pi^+\pi^0)/\mathcal{B}(D_s^+ \rightarrow K^+K^-\pi^+\pi^0)$ .

Sources	(a)	(b)	(c)
PID efficiency correction	1.7	...	1.7
Multiple-candidate selection	1.1	1.3	1.2
Signal parameterization	0.5	0.5	1.1
$M(D)$ resolution	0.5	...	1.4
Binning	0.6	0.5	0.7
Background $M^2(p_i p_j)$ distribution	0.1	0.1	0.3
Efficiency correction bias	0.6	0.8	1.1
Total uncertainty	2.3	1.9	3.0

As a correction accounting for the difference in particle identification (PID) efficiencies between data and MC is

included in Eq. (2), we evaluate the uncertainty on this correction. Signal and normalization modes differ by the flavor of at most one track in the final state. We evaluate the uncertainty introduced by this difference using a sample of  $D^{*+} \rightarrow D^0\pi^+$ ,  $D^0 \rightarrow K^-\pi^+$  decays. The resulting uncertainties are 0.9% for  $D^+ \rightarrow K^+K^-\pi^+\pi^0$  and 0.8% for  $D^+ \rightarrow K^-\pi^+\pi^+\pi^0$ ; 0.8% for  $D_s^+ \rightarrow K^+\pi^-\pi^+\pi^0$  and 0.9% for  $D_s^+ \rightarrow K^+K^-\pi^+\pi^0$ . We thus assign 1.7% as the systematic uncertainty for the ratios of their branching fractions.

We consider uncertainty arising from the multiple-candidate selection procedure by keeping all candidates without best candidate selection. We refit the  $M(D)$  distributions, redetermine the signal efficiency curves, and obtain the corrected yields with Eq. (2). The resulting changes in the branching fractions are assigned as systematic uncertainties.

The uncertainty due to PDF parameters that are fixed in the fit for a signal yield is evaluated by sampling these parameters from a multivariate Gaussian distribution that accounts for their uncertainties and correlations, and re-fitting for the signal yield. The procedure is repeated 1000 times, and the root-mean-square of the distribution of fitted yields is taken as the uncertainty due to the fixed parameters.

There are several sources of uncertainty in the efficiency correction procedure. We first consider effects due to the  $M(D)$  resolution. In Eq. (2), events satisfying  $|M(D) - m_D| < 20 \text{ MeV}/c^2$  were used; however, data and MC could have different mass resolutions, and this would bias the efficiency-corrected signal yield. We evaluate the efficiency of the signal region requirement ( $\varepsilon_{\text{SR}}$ ) by integrating the signal PDFs over this region. The ratio of the efficiency for a signal mode to that of a normalization mode is determined, both for data and MC. The ratio of these ratios  $[\varepsilon_{\text{SR}}^{\text{norm}}/\varepsilon_{\text{SR}}^{\text{sig}}(\text{data})]/[\varepsilon_{\text{SR}}^{\text{norm}}/\varepsilon_{\text{SR}}^{\text{sig}}(\text{MC})]$  is calculated, and the difference from unity is taken as the systematic uncertainty due to the  $M(D)$  resolution. These uncertainties are 0.5% for  $\mathcal{B}(D^+ \rightarrow K^+K^-\pi^+\pi^0)/\mathcal{B}(D^+ \rightarrow K^-\pi^+\pi^+\pi^0)$  and 1.4% for  $\mathcal{B}(D_s^+ \rightarrow K^+\pi^-\pi^+\pi^0)/\mathcal{B}(D_s^+ \rightarrow K^+K^-\pi^+\pi^0)$ . The uncertainty for  $\mathcal{B}(D^+ \rightarrow K^+\pi^-\pi^+\pi^0)/\mathcal{B}(D^+ \rightarrow K^-\pi^+\pi^+\pi^0)$  is negligible, as the final states have the same particles.

We also consider uncertainty due to binning. We repeat the efficiency correction with a different number of bins, e.g.,  $4 \times 4 \times 4 \times 4 = 1024$  bins for  $D^+ \rightarrow K^+K^-\pi^+\pi^0$ , and take the fractional change in the ratio of branching fractions as a systematic uncertainty.

We evaluate uncertainties arising from the 5D distribution of background events by applying a correction to the background distribution. This correction, obtained from MC, is the ratio of the background distribution for events having  $M(D)$  in the signal region to that for events having  $M(D)$  in the sideband. After applying this correction, the signal yield in each efficiency bin is recalculated. The fractional change in the overall efficiency-corrected

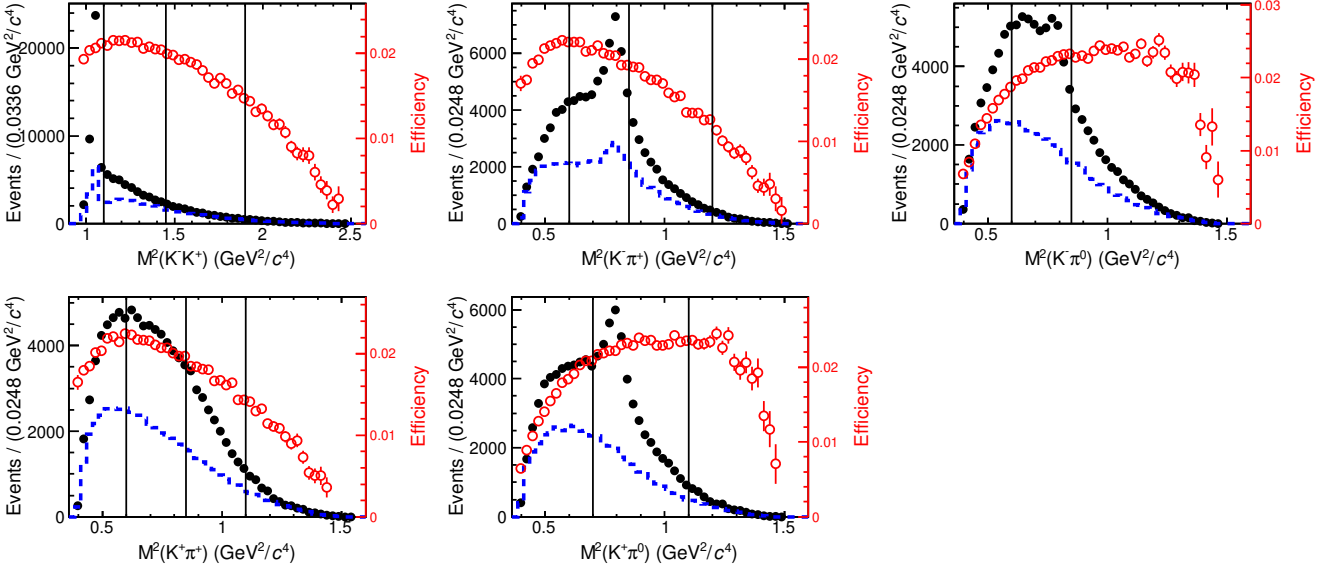


FIG. 4. Invariant-mass-squared distributions for different combinations of final-state particles (i.e., projections of the five-dimensional distribution) for  $D^+ \rightarrow K^+ K^- \pi^+ \pi^0$  decays. Events in the  $M(D)$  signal region are plotted as filled black circles; events in the  $M(D)$  sideband are plotted as blue dashed histograms; and signal efficiencies are plotted as red hollow circles. Black vertical lines denote the boundaries of the bins used for the efficiency correction.

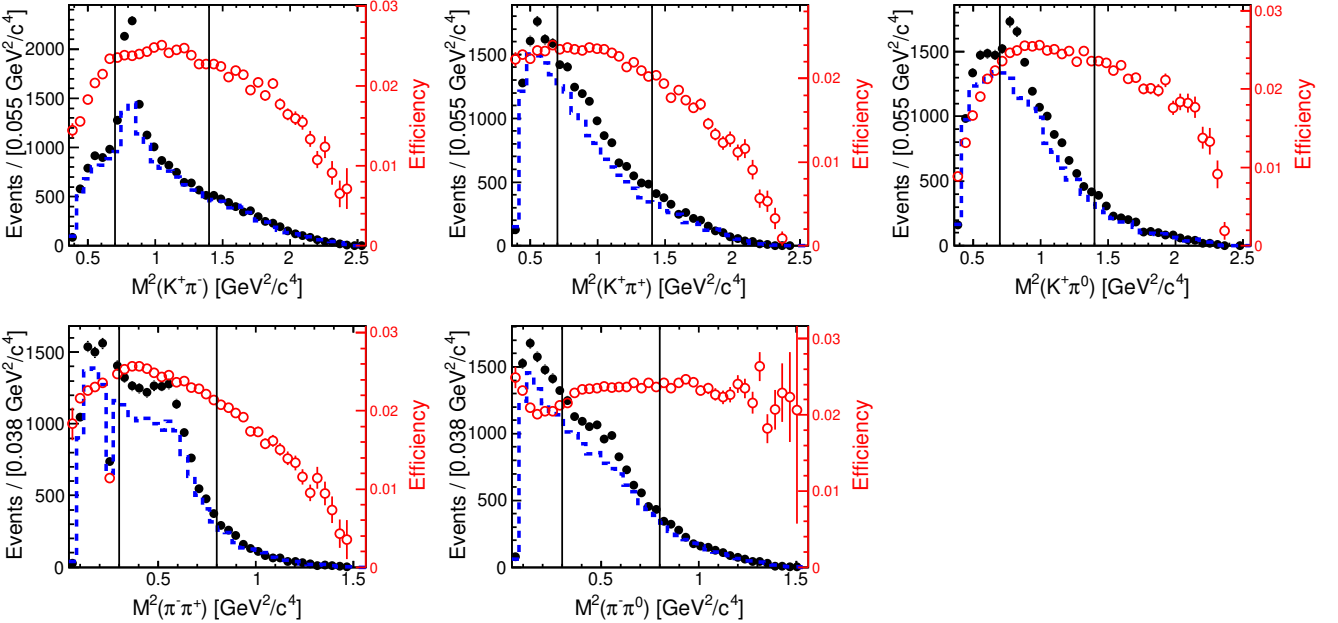


FIG. 5. Invariant-mass-squared distributions for different combinations of final-state particles for  $D^+ \rightarrow K^+ \pi^- \pi^+ \pi^0$  decays. Events in the  $M(D)$  signal region are plotted as filled black circles; events in the  $M(D)$  sideband are plotted as blue dashed histograms; and signal efficiencies are plotted as red hollow circles. Black vertical lines denote the boundaries of the bins used for the efficiency correction.

signal yield is assigned as a systematic uncertainty.

We check for bias in the efficiency correction due to possible intermediate resonances in the  $D^+$  or  $D_s^+$  decay, also using MC simulation. The results for the efficiency-corrected signal yields are all consistent with input values; the small differences observed are conservatively assigned as systematic uncertainties.

The total systematic uncertainty is obtained by summing all individual contributions in quadrature. The results are listed in Table II.

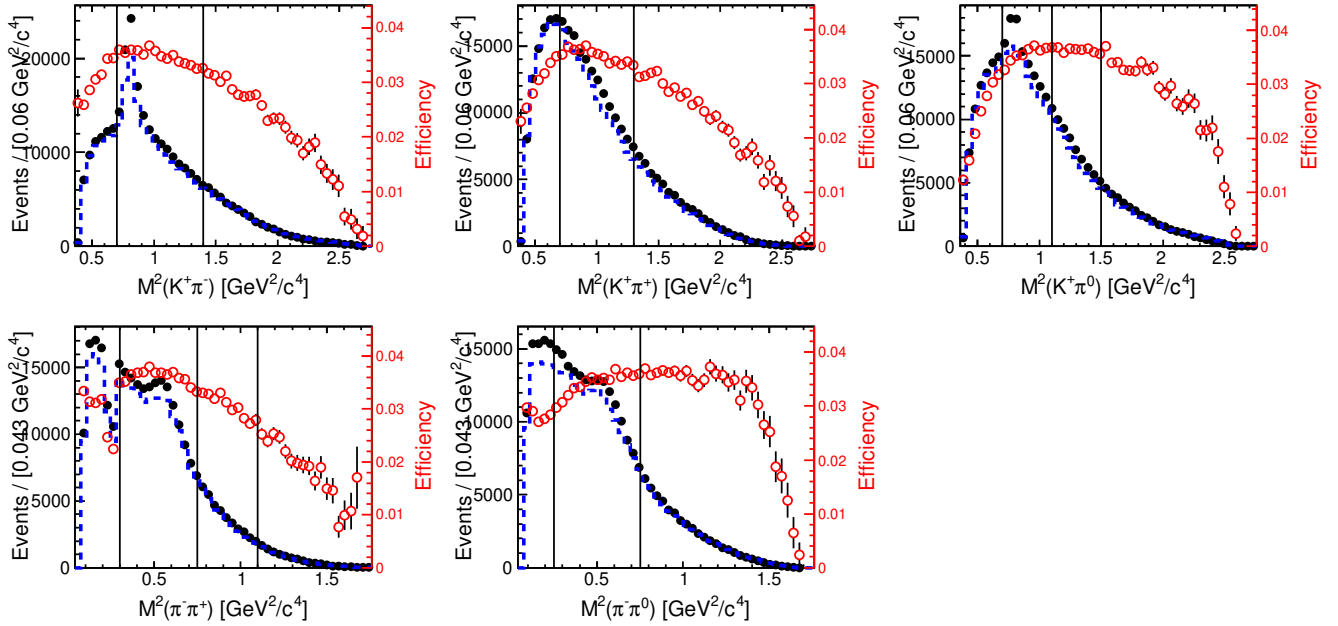


FIG. 6. Invariant-mass-squared distributions for different combinations of final-state particles for  $D_s^+ \rightarrow K^+ \pi^- \pi^+ \pi^0$  decays. Events in the  $M(D)$  signal region are plotted as filled black circles; events in the  $M(D)$  sideband are plotted as blue dashed histograms; and signal efficiencies are plotted as red hollow circles. Black vertical lines denote the boundaries of the bins used for the efficiency correction.

## VII. CONCLUSION

In summary, using  $980 \text{ fb}^{-1}$  of data collected with the Belle detector, we observe the SCS decays  $D^+ \rightarrow K^+ K^- \pi^+ \pi^0$  and  $D_s^+ \rightarrow K^+ \pi^- \pi^+ \pi^0$ , and the DCS decay  $D^+ \rightarrow K^+ \pi^- \pi^+ \pi^0$ . The statistical significance of each mode is greater than  $10\sigma$ . The branching fractions for these decays relative to the branching fractions for topologically similar CF decays are measured to be

$$\begin{aligned} \frac{\mathcal{B}(D^+ \rightarrow K^+ K^- \pi^+ \pi^0)}{\mathcal{B}(D^+ \rightarrow K^- \pi^+ \pi^+ \pi^0)} &= (11.32 \pm 0.13 \pm 0.26)\% \\ \frac{\mathcal{B}(D^+ \rightarrow K^+ \pi^- \pi^+ \pi^0)}{\mathcal{B}(D^+ \rightarrow K^- \pi^+ \pi^+ \pi^0)} &= (1.68 \pm 0.11 \pm 0.03)\% \\ \frac{\mathcal{B}(D_s^+ \rightarrow K^+ \pi^- \pi^+ \pi^0)}{\mathcal{B}(D_s^+ \rightarrow K^+ K^- \pi^+ \pi^0)} &= (17.13 \pm 0.62 \pm 0.51)\%, \end{aligned}$$

where the uncertainties are statistical and systematic, respectively. Taking  $\sin \theta_C = 0.2257$  [7], the second result above corresponds to  $(5.83 \pm 0.42) \times \tan^4 \theta_C$ . This value is significantly larger than other measured ratios of DCS to CF branching fractions, but it is consistent within  $1.2\sigma$  with the large rate of  $D^+ \rightarrow K^+ \pi^- \pi^+ \pi^0$  measured by BESIII [5, 6].

Inserting world average values for the branching fractions of the normalization modes  $\mathcal{B}(D^+ \rightarrow K^- \pi^+ \pi^+ \pi^0) = (6.25 \pm 0.18)\%$  [7] and  $\mathcal{B}(D_s^+ \rightarrow K^+ K^- \pi^+ \pi^0) = (5.51 \pm$

$0.19)\%$  [7, 18], we obtain

$$\begin{aligned} \mathcal{B}(D^+ \rightarrow K^+ K^- \pi^+ \pi^0) &= \\ &= (7.08 \pm 0.08 \pm 0.16 \pm 0.20) \times 10^{-3} \\ \mathcal{B}(D^+ \rightarrow K^+ \pi^- \pi^+ \pi^0) &= \\ &= (1.05 \pm 0.07 \pm 0.02 \pm 0.03) \times 10^{-3} \\ \mathcal{B}(D_s^+ \rightarrow K^+ \pi^- \pi^+ \pi^0) &= \\ &= (9.44 \pm 0.34 \pm 0.28 \pm 0.32) \times 10^{-3}, \end{aligned}$$

where the uncertainties are statistical, systematic, and from uncertainty in the branching fractions of the normalization modes, respectively. The first two results are consistent with recent BESIII results [4–6] but have greater precision. The last result is the first measurement of this Cabibbo-suppressed decay.

This work, based on data collected using the Belle detector, which was operated until June 2010, was supported by the Ministry of Education, Culture, Sports, Science, and Technology (MEXT) of Japan, the Japan Society for the Promotion of Science (JSPS), and the Tau-Lepton Physics Research Center of Nagoya University; the Australian Research Council including grants DP180102629, DP170102389, DP170102204, DE220100462, DP150103061, FT130100303; Austrian Federal Ministry of Education, Science and Research (FWF) and FWF Austrian Science Fund No. P 31361-N36; the National Natural Science Foundation of China under Contracts No. 11675166, No. 11705209; No. 11975076; No. 12135005; No. 12175041;

No. 12161141008; Key Research Program of Frontier Sciences, Chinese Academy of Sciences (CAS), Grant No. QYZDJ-SSW-SLH011; the Ministry of Education, Youth and Sports of the Czech Republic under Contract No. LTT17020; the Czech Science Foundation Grant No. 22-18469S; Horizon 2020 ERC Advanced Grant No. 884719 and ERC Starting Grant No. 947006 “Inter-Leptons” (European Union); the Carl Zeiss Foundation, the Deutsche Forschungsgemeinschaft, the Excellence Cluster Universe, and the VolkswagenStiftung; the Department of Atomic Energy (Project Identification No. RTI 4002) and the Department of Science and Technology of India; the Istituto Nazionale di Fisica Nucleare of Italy; National Research Foundation (NRF) of Korea Grant Nos. 2016R1D1A1B02012900, 2018R1A2B-3003643, 2018R1A6A1A06024970, RS202200197659, 2019R1I1A3A01058933, 2021R1A6A1A03043957, 2021R1F1A1060423, 2021R1F1A1064008, 2022R1A2C-1003993; Radiation Science Research Institute, Foreign Large-size Research Facility Application Supporting project, the Global Science Experimental Data Hub Center of the Korea Institute of Science and Technology Information and KREONET/GLORIAD; the Polish Ministry of Science and Higher Education and the National Science Center; the Ministry of Science and Higher Education of the Russian Federation, Agreement 14.W03.31.0026, and the HSE University Basic Research Program, Moscow; University of Tabuk research grants S-1440-0321, S-0256-1438, and S-0280-1439 (Saudi Arabia); the Slovenian Research Agency Grant Nos. J1-9124 and P1-0135; Ikerbasque, Basque Foundation for Science, Spain; the Swiss National Science Foundation; the Ministry of Education and the Ministry of Science and Technology of Taiwan; and the United States Department of Energy and the National Science Foundation. These acknowledgements are not to be interpreted as an endorsement of any statement made by any of our institutes, funding agencies, governments, or their representatives. We thank the KEKB group for the excellent operation of the accelerator; the KEK cryogenics group for the efficient operation of the solenoid; and the KEK computer group and the Pacific Northwest National Laboratory (PNNL) Environmental Molecular Sciences Laboratory (EMSL) computing group for strong computing support; and the National Institute of Informatics, and Science Information NETwork 6 (SINET6) for valuable network support.

- 
- [1] J. Brod, A. L. Kagan, and J. Zupan, *Phys. Rev. D* **86**, 014023 (2012).
  - [2] R. Aaij *et al.* (LHCb Collaboration), *Phys. Rev. Lett.* **122**, 211803 (2019).
  - [3] H.-Y. Cheng and C.-W. Chiang, *Phys. Rev. D* **81**, 074021 (2010).
  - [4] M. Ablikim *et al.* (BESIII Collaboration), *Phys. Rev. D* **102**, 052006 (2020).
  - [5] M. Ablikim *et al.* (BESIII Collaboration), *Phys. Rev. Lett.* **125**, 141802 (2020).
  - [6] M. Ablikim *et al.* (BESIII Collaboration), *Phys. Rev. D* **104**, 072005 (2021).
  - [7] P. A. Zyla *et al.* (Particle Data Group), *Prog. Theor. Exp. Phys.* **2020**, 083C01 (2020) and 2021 update.
  - [8] S. Kurokawa and E. Kikutani, *Nucl. Instrum. Methods Phys. Res. Sect. A* **499**, 1 (2003), and other papers included in this Volume; T. Abe *et al.*, *Prog. Theor. Exp. Phys.* **2013**, 03A001 (2013) and references therein.
  - [9] A. J. Bevan *et al.* (Belle and BaBar Collaborations), *Eur. Phys. J. C* **74** (2014) 3026.
  - [10] A. Abashian *et al.* (Belle Collaboration), *Nucl. Instrum. Methods Phys. Res. Sect. A* **479**, 117 (2002); also see Section 2 in J. Brodzicka *et al.*, *Prog. Theor. Exp. Phys.* **2012**, 04D001 (2012).
  - [11] D.J. Lange, *Nucl. Instrum. Methods Phys. Res. Sect. A* **462**, 152 (2001).
  - [12] R. Brun *et al.*, GEANT 3.21, CERN Report DD/EE/84-1, 1984.
  - [13] E. Barberio and Z. Was, *Comput. Phys. Commun.* **79** (1994) 291.
  - [14] E. Nakano, *Nucl. Instrum. Methods Phys. Res. Sect. A* **494**, 402 (2002).
  - [15] K. Hanagaki *et al.*, *Nucl. Instrum. Methods Phys. Res. Sect. A* **485** (2002) 490.
  - [16] A. Abashian *et al.*, *Nucl. Instrum. Methods Phys. Res. Sect. A* **491** (2002) 69.
  - [17] T. Skwarnicki, Ph.D Thesis, Institute for Nuclear Physics, Krakow 1986; DESY Internal Report, DESY F31-86-02 (1986).
  - [18] M. Ablikim *et al.* (BESIII Collaboration), *Phys. Rev. D* **104**, 032011 (2021).
  - [19] This parameterization assumes that the detector acceptance and reconstruction efficiency are independent of the signs of  $K$  and  $\pi$  momenta in the  $D$  rest frame (i.e., symmetric under a parity transformation). We have checked that any such dependence on the signs of momenta is negligible.